

# Non-linear multiphase flow in hydrophobic porous media

Yihuai Zhang<sup>1,\*</sup>, Branko Bijeljic<sup>1</sup>, and Martin J. Blunt<sup>1</sup>

<sup>1</sup>Department of Earth Science and Engineering, Imperial College London, London SW7 2BP, United Kingdom  
\*yihuai.zhang@imperial.ac.uk, this manuscript is a non-peer reviewed preprint submitted to EarthArXiv.

## ABSTRACT

Multiphase flow in porous materials is conventionally described by an empirical extension to Darcy's law which assumes that the pressure gradient is proportional to flow rate. Through a series of two-phase flow experiments, we demonstrate that even when capillary forces are dominant at the pore scale, there is a non-linear intermittent flow regime with a power-law dependence between pressure gradient and flow rate. Energy balance is used to predict accurately the start of the intermittent regime in hydrophobic porous media. The pore-scale explanation of the behaviour based on the periodic filling of critical flow pathways is confirmed through 3D micron-resolution X-ray imaging.

## Introduction

Multiphase flow in porous media occurs in a wide variety of natural and engineered settings, including carbon geosequestration, geoenery resources recovery, subsurface contaminant control, drug delivery and flow in fuel cells<sup>1-11</sup>. For the last 85 years multiphase flow has been quantified assuming that each fluid phase has its own pathway and the flow rate has linear relationship with pressure gradient, governed by an empirical extension of the Darcy law<sup>2,12,13</sup>,

$$q_i = -\frac{k_{ri}K}{\mu_i}(\nabla P_i - \rho_i g), \quad (1)$$

where  $q_i$  is the Darcy flux defined as the volume of phase  $i$  flowing per unit area per unit time,  $K$  is the absolute permeability of the sample,  $k_{ri}$  is the relative permeability,  $\mu_i$  is the viscosity,  $\nabla P_i$  is the pressure gradient for phase  $i$ , and  $\rho_i g$  is the contribution of gravity which is ignored in this study.

The capillary number  $Ca$  is defined as  $Ca = \mu q_t / \sigma$  where  $\mu$  is the average viscosity of the two fluids,  $q_t$  is the total Darcy flux of the two phases and  $\sigma$  is the interfacial tenasion. It is well known that  $Ca$  has a linear relationship with pressure gradient  $\nabla P$  at low flow rate,  $\nabla P \sim Ca$ <sup>1,2,14</sup>.

Recent research has shown that there is non-linear flow even at low capillary numbers where the capillary force is still dominant at the pore scale<sup>14-18</sup>. We observe a so-called intermittent regime with  $\nabla P \sim Ca^a$ ,  $1 > a > 0$ : the pressure gradient has a power-law relation with flow rate. At the pore scale, some regions of the void space, which provide additional connectivity, are intermittently occupied by both phases, as confirmed through high-resolution X-ray imaging and confocal microscopy<sup>14,19-23</sup>. This phenomenon is associated with non-thermal and non-periodic fluctuations in pressure and fluid occupancy representing a non-linear disordered dynamics<sup>24</sup>. Tallakstad et al.<sup>25</sup> was the first to observe this behaviour and suggested that  $a \approx 0.5$  from two-phase flow experiments in a quasi-two-dimensional porous medium. Sinha et al.<sup>26</sup> also proposed  $a = 0.5$  through an analysis of experiments and simulations. Gao et al.<sup>14</sup> found a threshold capillary number for the onset of intermittency  $Ca^i$  of approximately  $10^{-5}$  in two-phase steady-state flow tests on a water-wet (hydrophilic) sandstone sample with a water fractional flow (ratio of the volumetric flow rate of water to the total flow rate of oil and water)  $f_w = 0.5$ , where the exponent  $a$  was approximately 0.6. Recently, Zhang et al.<sup>1</sup> quantified the onset of intermittency as a function of fractional flow for different viscosity ratio fluids and rock types. To date, only two studies have investigated hydrophobic media (mixed-wet or oil-wet rocks) and have suggested that there may be more intermittency under these conditions<sup>27,28</sup>. However, there have been no quantitative studies of the onset of intermittency in non-water-wet systems.

In this paper, we conduct 174 steady-state immiscible two-phase core flooding experiments through an altered-wettability Bentheimer sandstone sample with different water fractional flows ( $f_w = 0.2, 0.4, 0.5, 0.6, 0.7$  and  $0.8$ ) where the capillary number varies from  $\sim 10^{-7}$  to  $\sim 10^{-4}$  during a waterflood displacement. We also performed high-resolution pore-scale imaging on a replicate sample for 14 flow rates and fractional flows covering both the linear and intermittent flow regimes. We use energy balance to predict accurately the boundary of the onset of intermittency which is consistent with our experimental results and *in situ* pore-scale X-ray images.

## Results

The results, for all water fractional flows  $f_w$ , clearly show that a transition from linear  $a = 1$  to a non-linear regime  $a < 1$  when the capillary number increases, Fig. 1. We found that the exponent  $a$  and threshold capillary number  $Ca^i$  are both functions of the fractional flow, see Table 1; the lowest value  $a = 0.50 \pm 0.01$  occurs when  $f_w = 0.4$ , indicating the strongest intermittency defined as the deviation from a linear Darcy law;  $f_w = 0.8$  had the highest exponent  $a = 0.58 \pm 0.01$  indicating weaker intermittency. The range of  $a$  is smaller when compared with similar experiments on a water-wet sample, where  $a$  varied from 0.44 to 0.74<sup>1</sup>. Moreover, the lower fractional flows have smaller threshold capillary numbers  $Ca^i$  for the onset of intermittency:  $Ca^i$  increased from  $10^{-5.7}$  to  $10^{-5.1}$  as the water fractional flow  $f_w$  increased from 0.2 to 0.8; this is the opposite trend to the water-wet results.

In the high resolution images, Fig. 2, it is evident that large pores are occupied by water as expected for media that are no longer water-wet<sup>14</sup>. We used the automated method to calculate contact angles directly on the images at the three-phase (oil-water-solid) contact line<sup>29</sup> for  $f_w = 0.5$ , 0.1 ml/min injection rate,  $Ca = 10^{-6}$ . The average contact angle is  $103^\circ$  with a standard deviation of  $22^\circ$ , representing a hydrophobic medium (mixed-wet or oil-wet)<sup>30</sup>.

At the pore scale it has been shown, in water-wet systems, that the non-linear flow behaviour is caused by intermittent filling of regions of the pore space alternately by both phases; the oil and water no longer travel through fixed flow pathways at steady state. We use our images to quantify regions of the pore space that are always occupied by oil during the scan time of 1 hour, always occupied by water, and intermittent regions, identified by intermediate greyscale values, which are occupied by both oil and water during the scan time. As an example, Fig. 2 shows that there is more intermittency for the lower water fractional flows, consistent with the threshold capillary numbers and exponents listed in Table 1. Fig. 3 demonstrates how the degree of intermittency increases with flow rate. In the Darcy regime, the volume of any intermittent regions is negligible and the two phases flow through fixed flow pathways. In the intermittent regime, a significant fraction of the pore space is periodically occupied by both phases, facilitating flow; more pathways open up as the capillary number increases, leading to a non-linear relationship between flow rate and pressure gradient.

## Discussion

We now quantify the onset of intermittency using an energy balance argument. We generalize our previous work<sup>1</sup> by identifying oil as the wetting phase and water as non-wetting. Intermittency first occurs when the energy to create an interface in a pore of typical radius  $r$ ,  $\sigma r^2$  is approximately equal to the work done to inject fluid in a characteristic pore length  $l$ ,  $\phi l^4 \nabla P$ , where  $\nabla P$  is the pressure gradient and  $\phi$  is the porosity. To estimate the pressure gradient, we assume Darcy-like flow with a total flow rate  $q_t^i$  and a limiting mobility  $f_w/\mu_{nw}$ , controlled by the flow of the non-wetting phase (water) displacing the wetting phase (oil) with an effective relative permeability, at least in the viscous-flow limit of  $f_w$ . Hence from Eq. (1) we estimate  $\nabla P \approx -\mu_{nw} q_t^i / K f_w$ . We then expect the onset of intermittency when:

$$\sigma r^2 = \frac{\mu_{nw} q_t^i \phi l^4}{K f_w}. \quad (2)$$

This can be rearranged to write the threshold water (non-wetting) phase capillary number  $Ca_w^i = \mu_w f_w q_t^i / \sigma$  and oil (wetting) phase capillary number  $Ca_{nw}^i = \mu_{nw} (1 - f_w) q_t^i / \sigma$  as follows:

$$Ca_w^i = Y^i (f_w)^2, \quad (3)$$

and

$$Ca_{nw}^i = Y^i f_w (1 - f_w) \frac{\mu_{nw}}{\mu_w}, \quad (4)$$

and the dimensionless number  $Y^i$  is defined by:

$$Y^i = \frac{\mu_w}{\mu_{nw}} \frac{K r^2}{\phi l^4}. \quad (5)$$

For Bentheimer sandstone, the mean pore radius  $r$  is  $24 \mu\text{m}$ <sup>2</sup> and  $l$  has a value of approximately  $150 \mu\text{m}$ <sup>14</sup> which is the mean pore-to-pore distance obtained from pore-network analysis<sup>31</sup>. Then we calculate  $Y^i$  to be  $\approx 10^{-5}$ .

In Fig. 4, our results for sample A (Table 1) are plotted on a phase diagram as a function of  $Ca_w$  and  $Ca_{nw}$ <sup>23</sup>. Eqs. (3) and (4) accurately predict the onset of intermittency for all fractional flows.

Furthermore, we quantify the fraction of the pore space that is intermittently occupied based on the pore-scale images for Sample B, Fig. 5. In the Darcy regime, it has zero intermittent phase or the small amount of intermittent occupancy that is

insufficient to perturb the linear Darcy law<sup>14</sup>; once non-linear behaviour emerges the fraction of the pore space periodically occupied by both phases increases up to 28% in the cases studied. In Fig. 5, we also show a good agreement between our theory and previously published work for mixed-wet Bentheimer sandstone from Zou et al.<sup>28</sup>, with a different viscosity ratio (the oil-water viscosity ratio was 1.46), where the three experiments are all in the predicted intermittent regime or near the threshold line. It should be noted that in previous work we showed that the energy balance theory also accurately predicted the onset of intermittency for a wide range of data in the literature on water-wet samples for different rock types and viscosity ratios<sup>1</sup>.

We have measured the pressure gradient and imaged the non-linear pore scale dynamics as a function of capillary number for different water fractional flows on hydrophobic porous media with a wide range of local contact angle during steady-state immiscible two-phase displacement. The Darcy flow regime and the transition to intermittent flow regime have been observed. Using energy balance, we have proposed the threshold line for the onset of intermittent flow, Eqs. (3) and (4), which accurately matches the experimental results and pore scale images. The work provides a quantification of non-linear flow which is likely to be encountered in many processes, including carbon dioxide storage, subsurface gas production, and in manufactured devices in fuel cells, micro-fluidics devices used in drug delivery and catalysis which involve multiphase fluid flow in porous media.

## Methods

We have studied two Bentheimer sandstone samples (Samples A and B, drilled from the same block). First the samples were completely saturated with brine; then crude oil from the Middle East was injected and then the samples were left in the crude oil for two months at 80°C temperature and 3 MPa pressure. Direct contact of the crude oil with parts of the solid surface altered the wettability from water-wet to a more mixed-wet to oil-wet state<sup>30,32</sup>. Decane was injected at 3 ml/min for 60 mins to replace the crude oil. The absolute permeability of the samples was measured during single-phase brine flow to be  $K = 1.85(\pm 0.02) \times 10^{-12} \text{ m}^2$ . Sample A (5.97 mm diameter and 27.88 mm length) was mounted in a specially designed core flooding system<sup>14,21</sup>. The water (brine) phase was 15 wt% KI (potassium iodide) brine, and the oil phase was *n*-decane, both injected by high precision ISCO pumps through a dual injection port<sup>1</sup>. The measured viscosity of the brine  $\mu_w = 0.821 \text{ mPas}$ , the *n*-decane viscosity  $\mu_{nw} = 0.838 \text{ mPas}$  (PubChem, open chemistry database), while the interfacial tension was measured to be  $\sigma = 47 \text{ mN/m}$ .

During experiments, a high-precision pressure transducer, Keller PD-33, recorded the pressure difference between the inlet and outlet of the sample. Similar to the experimental protocol in Zhang et al.<sup>1</sup>, we started the two-phase flow experiment from a low water fractional flow and low flow rate:  $f_w$  of 0.2 at 0.02 ml/min total flow rate ( $Ca = 2.1 \times 10^{-7}$ ); the pressure gradient was recorded after 12 hours when it stabilized, and then the flow rate increased from low to high and the pressure gradients at steady-state were recorded; 29 flow rates were considered for each  $f_w$ : the highest flow rate was 4.5 ml/min ( $Ca = 4.8 \times 10^{-5}$ ). Note that the time for the pressure gradient to stabilize depended on the flow rate: it was up to 12 hours for the low flow rate (0.02 ml/min), while as little as 5 minutes for the highest rates (greater than 3 ml/min). *n*-decane was injected at 3 ml/min for 30 mins again to return to the initial saturation after each sequence of experiments at the same fractional flow. We repeated this injection sequence for other fractional flows: 0.4, 0.5, 0.6, 0.7, and 0.8; in total 174 flow experiments were conducted.

For Sample B (6.15 mm diameter and 50.13 mm length), we have followed the same core flooding experiments protocol as for Sample A but replaced the water phase with 30 wt% KI (potassium iodide) brine for a better X-ray contrast; the viscosity of the brine was measured as 0.819 mPas<sup>33</sup>. The core flooding system was placed in a Zeiss XRM-510 X-ray microscope for high resolution *in situ* imaging<sup>30,33-35</sup>. The scan setting was 3.58  $\mu\text{m}$  voxel size, 0.5 s exposure time, 75 kV X-ray energy, 1601 projections with a flat panel detector. The scan time was around 1 hour. We selected and repeated 14 test points: 0.1, 0.2, 0.8 ml/min flow rates for  $f_w = 0.2$ ; 0.1, 0.2, 0.8, 1.25 ml/min flow rates for  $f_w = 0.5$ ; 0.1, 0.2, 0.8, 1.25 ml/min for  $f_w = 0.7$ ; and 0.1, 0.2, 0.8 ml/min flow rates for  $f_w = 0.8$ .

## References

1. Zhang, Y., Bijeljic, B., Gao, Y., Lin, Q. & Blunt, M. J. Quantification of nonlinear multiphase flow in porous media. *Geophys. Res. Lett.* **48**, e2020GL090477 (2021).
2. Blunt, M. J. *Multiphase flow in permeable media: A pore-scale perspective* (Cambridge University Press, 2017).
3. Gjennestad, M. A., Winkler, M. & Hansen, A. Pore network modeling of the effects of viscosity ratio and pressure gradient on steady-state incompressible two-phase flow in porous media. *Transp. Porous Media* 1–25 (2020).
4. Pak, T., Butler, I. B., Geiger, S., van Dijke, M. I. & Sorbie, K. S. Droplet fragmentation: 3d imaging of a previously unidentified pore-scale process during multiphase flow in porous media. *Proc. Natl. Acad. Sci.* **112**, 1947–1952 (2015).
5. Reynolds, C. & Krevor, S. Characterizing flow behavior for gas injection: Relative permeability of co2-brine and n2-water in heterogeneous rocks. *Water Resour. Res.* **51**, 9464–9489 (2015).

6. Zhang, Y., Lebedev, M., Jing, Y., Yu, H. & Iglauer, S. In-situ x-ray micro-computed tomography imaging of the microstructural changes in water-bearing medium rank coal by supercritical co<sub>2</sub> flooding. *Int. J. Coal Geol.* **203**, 28–35 (2019).
7. Zhao, B., Pahlavan, A. A., Cueto-Felgueroso, L. & Juanes, R. Forced wetting transition and bubble pinch-off in a capillary tube. *Phys. review letters* **120**, 084501 (2018).
8. Gao, Y., Raeini, A. Q., Blunt, M. J. & Bijeljic, B. Dynamic fluid configurations in steady-state two-phase flow in bentheimer sandstone. *Phys. Rev. E* **103**, 013110 (2021).
9. Iglauer, S. *et al.* Residual trapping of co<sub>2</sub> in an oil-filled, oil-wet sandstone core: Results of three-phase pore-scale imaging. *Geophys. Res. Lett.* **46**, 11146–11154 (2019).
10. Berg, S. *et al.* Real-time 3d imaging of haines jumps in porous media flow. *Proc. Natl. Acad. Sci.* **110**, 3755–3759 (2013).
11. Zhao, B. *et al.* Comprehensive comparison of pore-scale models for multiphase flow in porous media. *Proc. Natl. Acad. Sci.* **116**, 13799–13806 (2019).
12. Muskat, M. & Meres, M. W. The flow of heterogeneous fluids through porous media. *Physics* **7**, 346–363 (1936).
13. Muskat, M. The flow of homogeneous fluids through porous media. *Soil Sci.* **46**, 169 (1938).
14. Gao, Y., Lin, Q., Bijeljic, B. & Blunt, M. J. Pore-scale dynamics and the multiphase darcy law. *Phys. Rev. Fluids* **5**, 013801 (2020).
15. Armstrong, R. T. & Berg, S. Interfacial velocities and capillary pressure gradients during haines jumps. *Phys. Rev. E* **88**, 043010 (2013).
16. Rücker, M. *et al.* From connected pathway flow to ganglion dynamics. *Geophys. Res. Lett.* **42**, 3888–3894 (2015).
17. Rassi, E. M., Codd, S. L. & Seymour, J. D. Nuclear magnetic resonance characterization of the stationary dynamics of partially saturated media during steady-state infiltration flow. *New J. Phys.* **13**, 015007 (2011).
18. Sinha, S. & Hansen, A. Effective rheology of immiscible two-phase flow in porous media. *EPL (Europhysics Lett.)* **99**, 44004 (2012).
19. Spurin, C., Bultreys, T., Bijeljic, B., Blunt, M. J. & Krevor, S. Intermittent fluid connectivity during two-phase flow in a heterogeneous carbonate rock. *Phys. Rev. E* **100**, 043103 (2019).
20. Spurin, C., Bultreys, T., Bijeljic, B., Blunt, M. J. & Krevor, S. Mechanisms controlling fluid breakup and reconnection during two-phase flow in porous media. *Phys. Rev. E* **100**, 043115 (2019).
21. Gao, Y., Lin, Q., Bijeljic, B. & Blunt, M. J. X-ray microtomography of intermittency in multiphase flow at steady state using a differential imaging method. *Water resources research* **53**, 10274–10292 (2017).
22. Reynolds, C. A., Menke, H., Andrew, M., Blunt, M. J. & Krevor, S. Dynamic fluid connectivity during steady-state multiphase flow in a sandstone. *Proc. Natl. Acad. Sci.* **114**, 8187–8192 (2017).
23. Datta, S. S., Dupin, J.-B. & Weitz, D. A. Fluid breakup during simultaneous two-phase flow through a three-dimensional porous medium. *Phys. Fluids* **26**, 062004 (2014).
24. Rücker, M. *et al.* The origin of non-thermal fluctuations in multiphase flow in porous media. *Front. Water* **3**, 45 (2021).
25. Tallakstad, K. T. *et al.* Steady-state two-phase flow in porous media: statistics and transport properties. *Phys. review letters* **102**, 074502 (2009).
26. Sinha, S. *et al.* Effective rheology of two-phase flow in three-dimensional porous media: experiment and simulation. *Transp. porous media* **119**, 77–94 (2017).
27. Rücker, M. *et al.* The effect of mixed wettability on pore-scale flow regimes based on a flooding experiment in ketton limestone. *Geophys. Res. Lett.* **46**, 3225–3234 (2019).
28. Zou, S., Armstrong, R. T., Arns, J.-Y., Arns, C. H. & Hussain, F. Experimental and theoretical evidence for increased ganglion dynamics during fractional flow in mixed-wet porous media. *Water Resour. Res.* **54**, 3277–3289 (2018).
29. AlRatrou, A., Raeini, A. Q., Bijeljic, B. & Blunt, M. J. Automatic measurement of contact angle in pore-space images. *Adv. Water Resour.* **109**, 158–169 (2017).
30. Lin, Q. *et al.* Minimal surfaces in porous media: Pore-scale imaging of multiphase flow in an altered-wettability bentheimer sandstone. *Phys. Rev. E* **99**, 063105 (2019).
31. Raeini, A. Q., Bijeljic, B. & Blunt, M. J. Generalized network modeling: Network extraction as a coarse-scale discretization of the void space of porous media. *Phys. Rev. E* **96**, 013312 (2017).

32. Lin, Q., Bijeljic, B., Foroughi, S., Berg, S. & Blunt, M. J. Pore-scale imaging of displacement patterns in an altered-wettability carbonate. *Chem. Eng. Sci.* **235**, 116464 (2021).
33. Gao, Y., Raeini, A. Q., Blunt, M. J. & Bijeljic, B. Pore occupancy, relative permeability and flow intermittency measurements using x-ray micro-tomography in a complex carbonate. *Adv. Water Resour.* **129**, 56–69 (2019).
34. Lebedev, M. *et al.* Carbon geosequestration in limestone: Pore-scale dissolution and geomechanical weakening. *Int. J. Greenh. Gas Control.* **66**, 106–119 (2017).
35. Zhang, Y., Lebedev, M., Sarmadivaleh, M., Barifcani, A. & Iglauer, S. Swelling-induced changes in coal microstructure due to supercritical co2 injection. *Geophys. Res. Lett.* **43**, 9077–9083 (2016).

## Acknowledgements

We gratefully acknowledge funding from the Shell Digital Rocks programme at Imperial College London. We are grateful to Dr. Steffen Berg for many useful discussions on this work.

## Author contributions statement

Y.Z. conceived the ideas, conducted the experiments, and analysed the results. B.B. conceived the ideas supervised the projects. M.B. conceived the ideas supervised the projects. All authors reviewed the manuscript.

## Additional information

The authors declare no competing interests.

**Table 1.** Summary of the exponent  $a$  for  $\nabla P \sim Ca^a$ , threshold capillary number  $Ca^i$  for the onset of intermittency, and the associated oil phase capillary number  $Ca_{nw}^i$ , water phase capillary number  $Ca_w^i$ , from Fig. 1.

Fractional flow ( $f_w$ )	Exponent $a$ ( $Ca < Ca^i$ )	$Ca^i$	$Ca_{nw}^i$	$Ca_w^i$	Exponent $a$ ( $Ca > Ca^i$ )
0.2	1	$\sim 10^{-5.7}$	$\sim 10^{-5.8}$	$\sim 10^{-6.4}$	$0.55 \pm 0.01$
0.4	1	$\sim 10^{-5.4}$	$\sim 10^{-5.6}$	$\sim 10^{-5.8}$	$0.50 \pm 0.01$
0.5	1	$\sim 10^{-5.3}$	$\sim 10^{-5.6}$	$\sim 10^{-5.6}$	$0.51 \pm 0.01$
0.6	1	$\sim 10^{-5.2}$	$\sim 10^{-5.6}$	$\sim 10^{-5.4}$	$0.56 \pm 0.01$
0.7	1	$\sim 10^{-5.1}$	$\sim 10^{-5.7}$	$\sim 10^{-5.3}$	$0.57 \pm 0.01$
0.8	1	$\sim 10^{-5.1}$	$\sim 10^{-5.8}$	$\sim 10^{-5.2}$	$0.58 \pm 0.01$

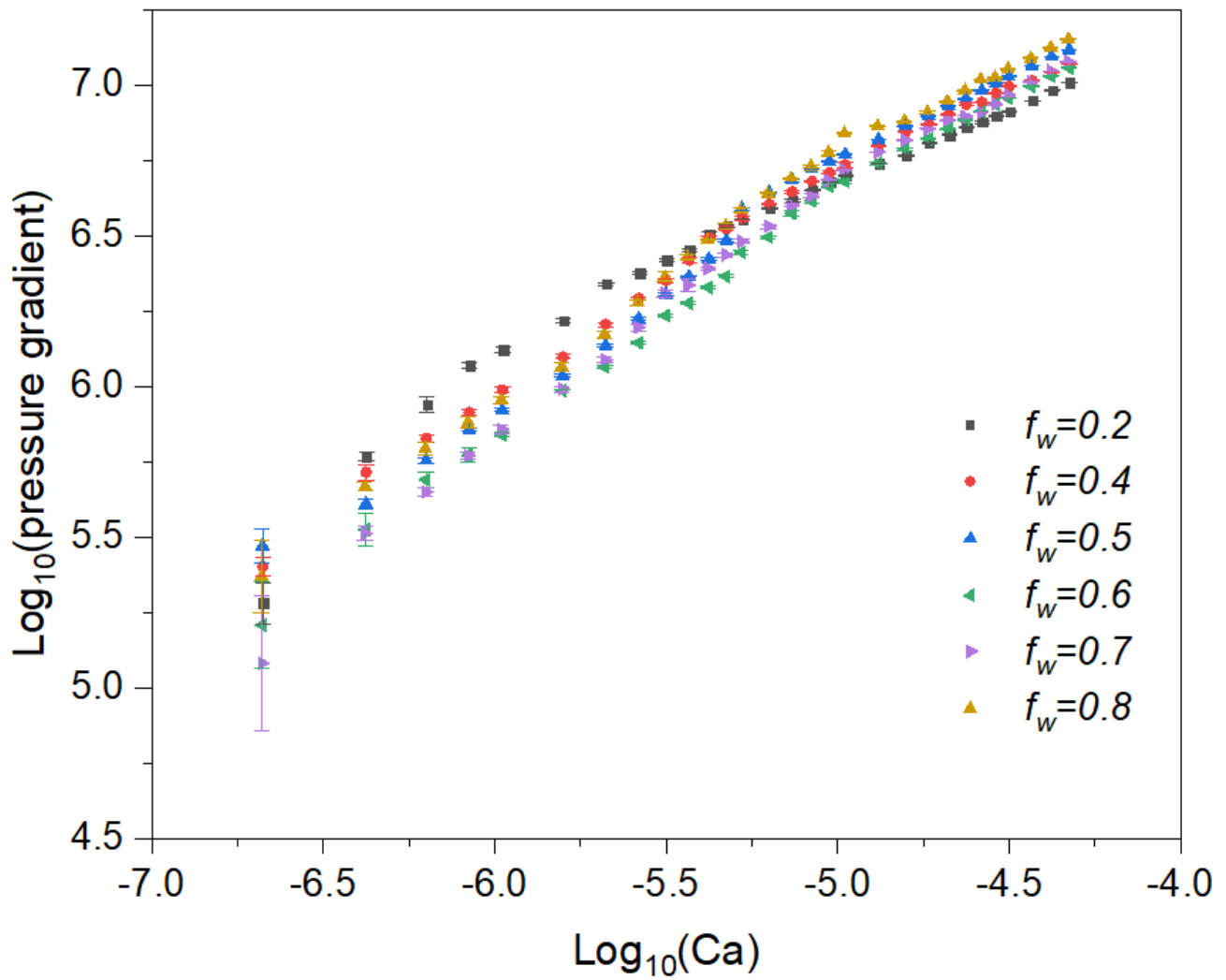


**Figure 1.** Summary of the measured pressure gradient  $\nabla P$  as a function of capillary number  $Ca$ , for different water fractional flows  $f_w$ : 0.2, 0.4, 0.5, 0.6, 0.7, and 0.8.

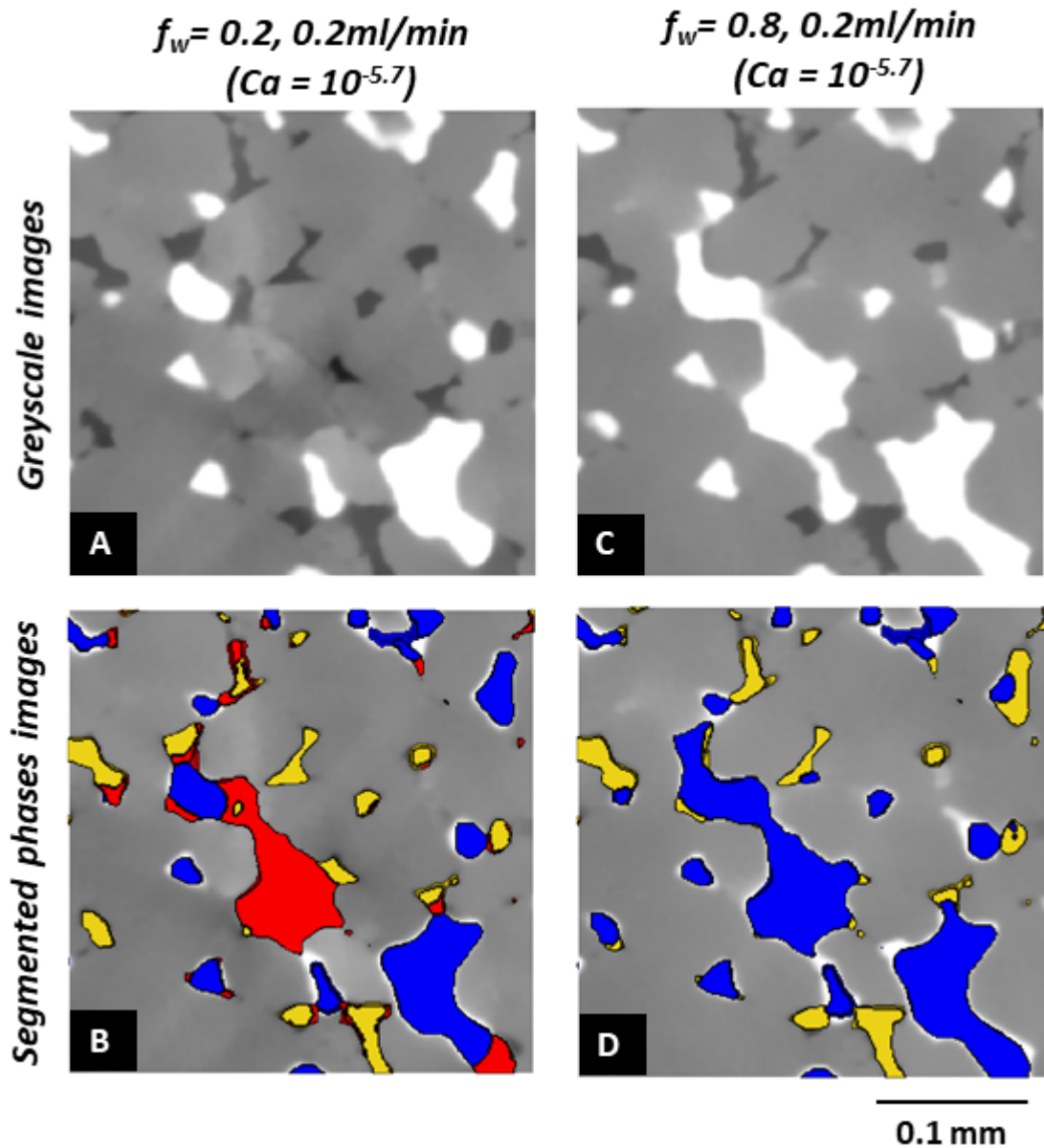


**Figure 2.** Example phase configurations in the same area of the rock sample at the same flow rate (0.2 ml/min) but different water fractional flows:  $f_w = 0.2$  and  $0.8$ ; the capillary number is  $10^{-5.7}$ . (A) and (C) are greyscale images. (B) and (D) are segmented images where blue is water, yellow is oil and red represents intermittent regions that were periodically occupied by both oil and water during the 1 hour scan time..

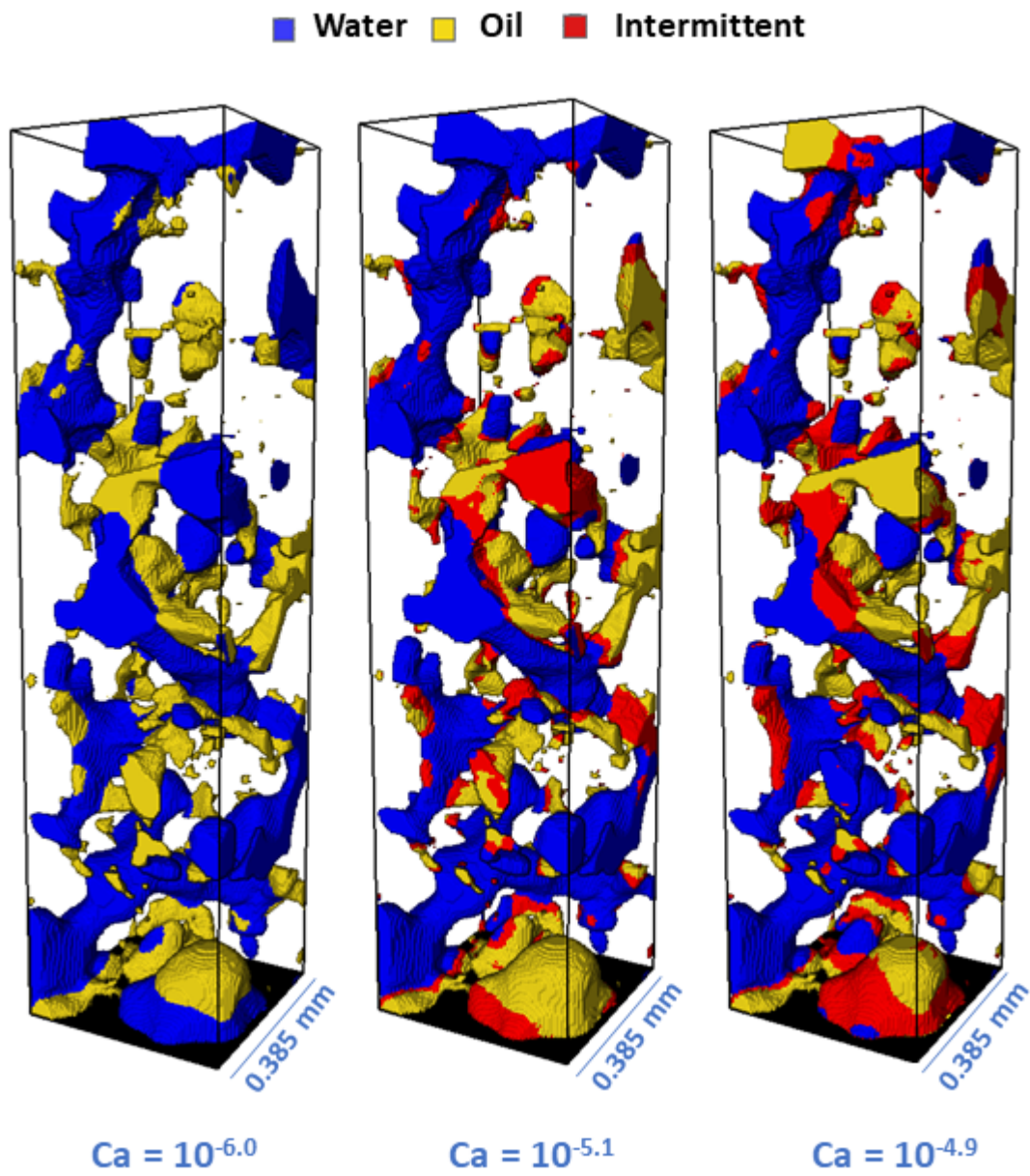


**Figure 3.** 3D views of the segmented phases on a  $100 \times 100 \times 400$  voxels sub-volume of the full image for  $f_w = 0.7$  and  $Ca = 10^{-6.0}, 10^{-5.1}, 10^{-4.9}$ . Water is blue, oil is yellow and intermittent regions are shown in red.

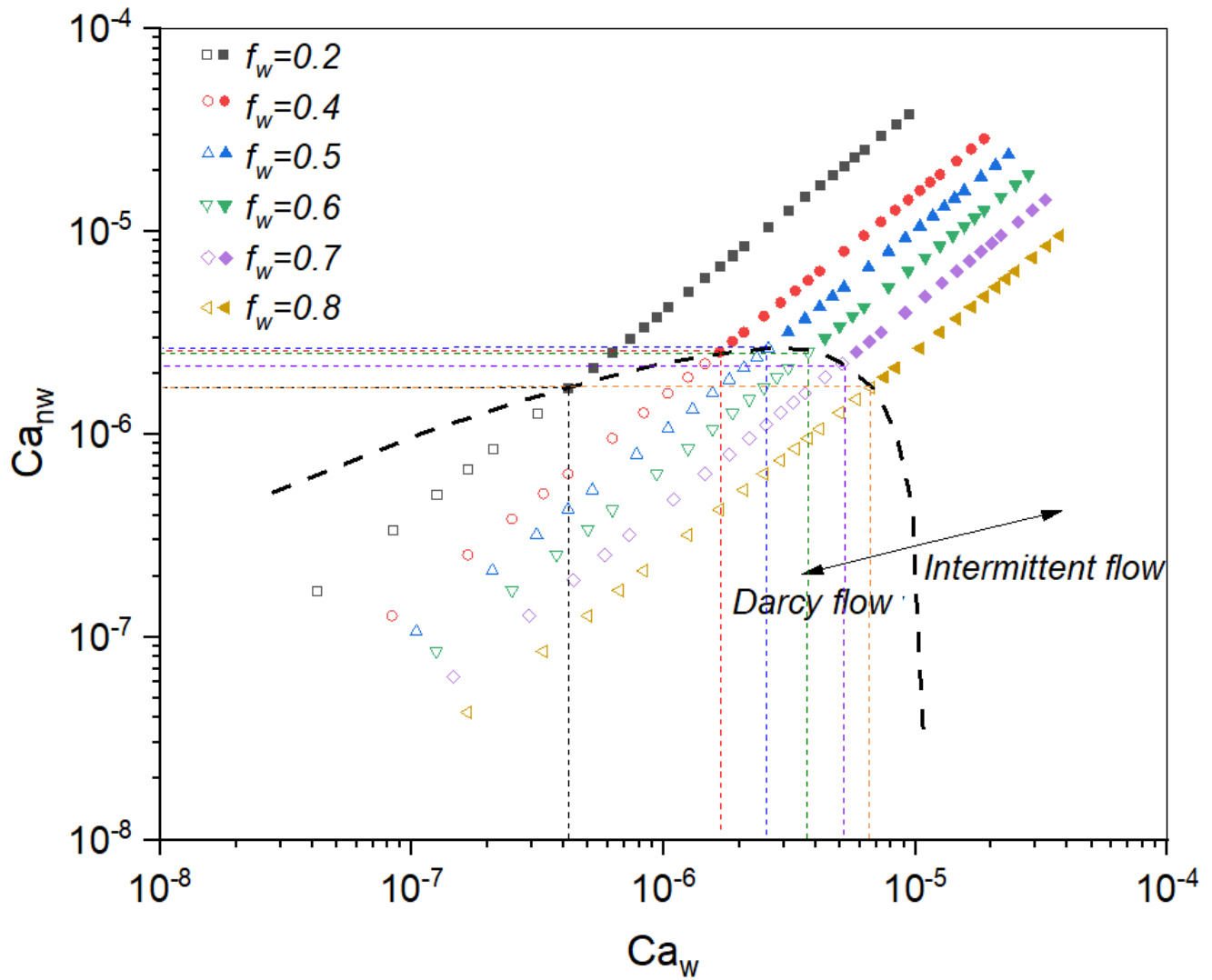


**Figure 4.** The phase diagram of the linear flow (empty symbols) points and non-linear flow (filled symbols) points for Sample A as a function of oil capillary number  $Ca_{nw}^i$  and water capillary number  $Ca_w^i$ . The dashed line is the predicted threshold line transition from Darcy to intermittent flow using Eqs. (3) and (4).

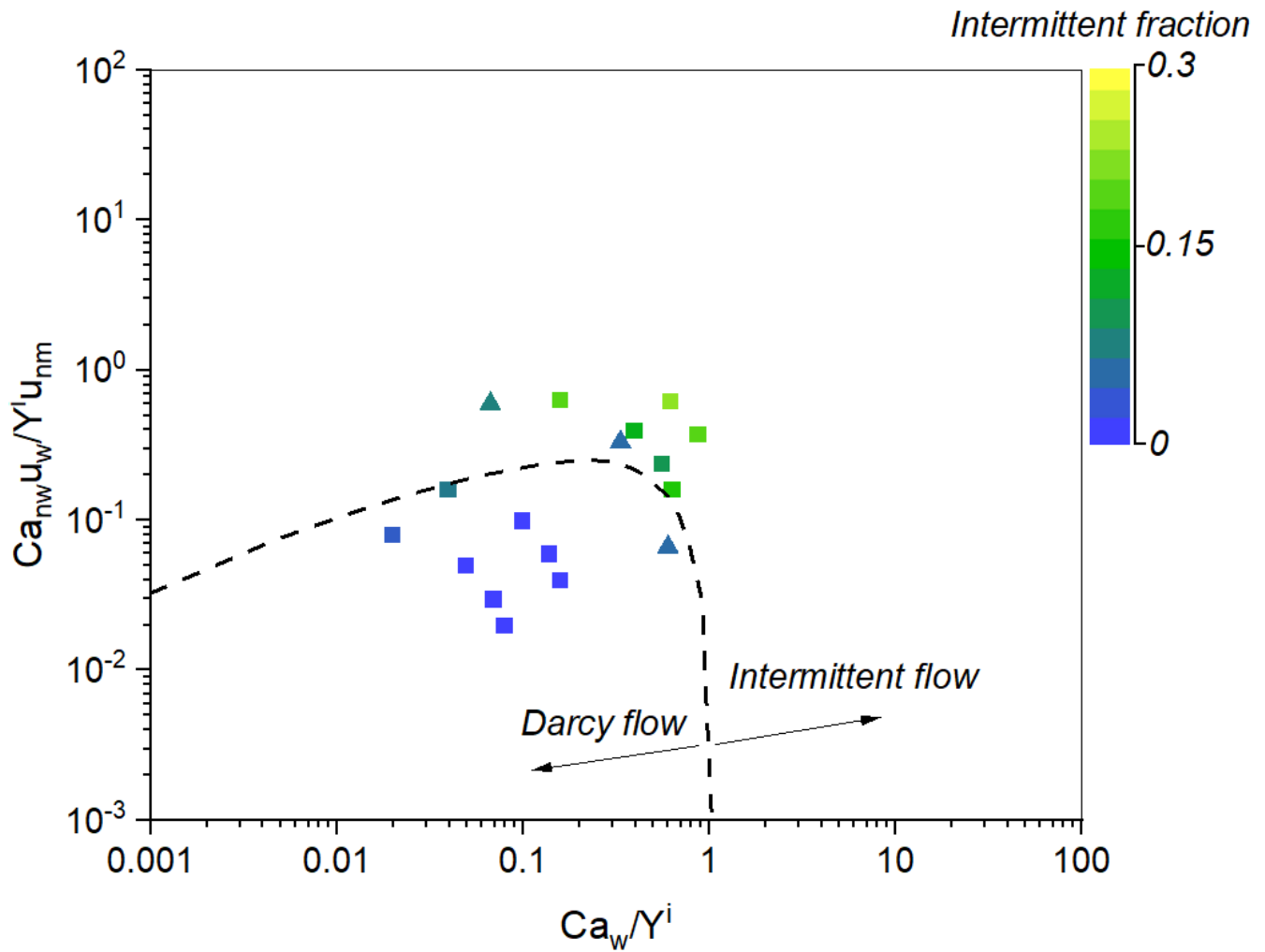


**Figure 5.** The re-plotted phase diagram showing the fraction of the pore space that has intermittent occupancy; the squares are for Sample B, and the triangles are data from the literature<sup>28</sup>. The dashed line is the predicted threshold line transition from Darcy to intermittent flow using Eqs. (3) and (4).